Journal of the Korean Nuclear Society
Volume 33, Number 2, pp.132~144, April, 2001

Treatment of Stainless Steel Cladding in Pressurized Thermal Shock Evaluation: Deterministic Analyses

Changheui Jang, Ill-Seok Jeong, and Sung-Yull Hong
Korea Electric Power Research Institute
103-16 Munji-dong, Yusong-gu, Daejon, Korea 305-380
chjang@kepri.re.kr

(Received February 21, 2000)

Abstract

Fracture mechanics is one of the major areas of the pressurized thermal shock (PTS) evaluation. To evaluate the reactor pressure vessel integrity associated with PTS, PFM methodology demands precise calculation of temperature, stress, and stress intensity factor for the variety of PTS transients. However, the existence of stainless steel cladding, with different thermal, physical, and mechanical property, at the inner surface of reactor pressure vessel complicates the fracture mechanics analysis. In this paper, treatment schemes to evaluate stress and resulting stress intensity factor for RPV with stainless steel clad are introduced. For a reference transient, the effects of clad thermal conductivity and thermal expansion coefficients on deterministic fracture mechanics analysis are examined.

Key Words : pressurized thermal shock, deterministic analysis, reactor pressure vessel, cladding effects, stress analysis, stress intensity factors, critical RT_{NDT}.

1. Introduction

During the operation of pressurized water reactor, certain type of transients could induce rapid cooldown of reactor pressure vessel (RPV) with relatively high or increasing system pressure. This type of transients was named as "Pressurized Thermal Shock (PTS)" to distinguish it from the conventional definition of thermal shock which only considered rapid cooling of RPV[1]. Unlike thermal shock events, the combination of thermal and pressure stress could substantially raise the possibility of rapid non-ductile failure of, especially highly embrittled RPVs with flaws.

For the quantitative evaluation of the vessel failure risk associated with PTS, the probabilistic fracture mechanics (PFM) analysis technique has been used[2,3,4]. Though PFM requires a lot of input parameters and fair amount of calculation, it basically checks whether hypothetical flaws within the wall propagate through the vessel by comparing applied stress intensity factor with fracture toughness (materials resistance to fracture) during the PTS events. Therefore, accurate calculation of applied stress intensity factor at the crack tip is as important as the sampling schemes

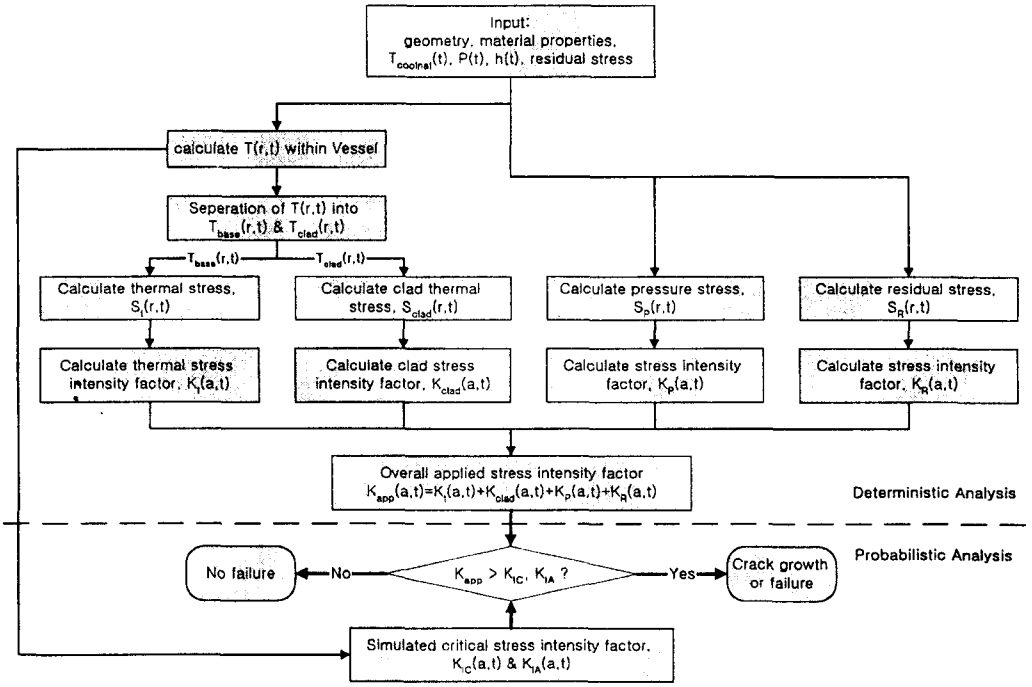

Fig. 1. Schematics of the Probabilistic Fracture Mechanics Analysis Procedure

of variety of parameters including fracture toughness by Monte Carlo simulation.

The overall flow of calculating the applied stress intensity factor is shown in figure 1. To calculate the applied stress intensity factors at the crack tip, individual stress intensity factor from all stress components should be separately evaluated. This approach was previously employed in VISA-II code developed by PNL with NRC sponsorship[3]. The advantage of this approach is that the contribution of each stress components can be easily quantified. Also, if each stress component can be depicted as analytical functional form, corresponding stress intensity factor can be easily calculated using influence coefficients[3,5,6].

Most RPVs of pressurized water reactors are made of carbon steels. And, inside surfaces of RPVs are clad with corrosion resistant materials, such as stainless steels and/or inconels to prevent general corrosion. Stainless steels and inconels have quite different thermal, physical, and mechanical properties from carbon steels. Especially, the differences in thermal conductivity and thermal expansion coefficients between the clad and base could affect the temperature and stress distribution within the vessel wall. Lower thermal conductivity of clad could generate steeper temperature gradient within clad with moderate gradient in base. Larger thermal expansion of clad could generate even larger thermal stress within the clad. Eventually, this stress distribution could have significant impact on the stress intensity factor at the crack tip.

Recently, the importance of treatment scheme of cladding in PTS analysis has been emphasized and need for improvement has been raised in comparative study of existing PFM codes[7]. In this paper, treatment schemes to evaluate thermal

stress and resulting stress intensity factor for RPV with stainless steel clad are introduced. And for a reference transient, the effects of clad thermal conductivity and thermal expansion coefficient on deterministic analysis of PTS are examined.

2. Methodology

2.1. Thermal Analysis

The beltline region of RPV is sufficiently far away from the nozzle area as well as the upper and lower heads to be treated as axisymmetric infinite cylindrical shell during the heat transfer/conduction analysis. In an axisymmetric infinite cylinder, heat transfer occurs only in r-direction. This can considerably simplify the analysis. Convective boundary condition and unsteady heat conduction equations given in eq. 1) and 2) should be solved to find the time dependent temperature profile, T(r,t).

$$-k(t)\cdot\left.\frac{T(r,t)}{\partial r}\right|_{wall} = h(t)\cdot(T_{wall}(t)-T_{\infty}(t)) \quad (1)$$

at the inner surface (r = R_i)

$$\frac{1}{r}\frac{\partial}{\partial r}\left(r\frac{\partial T(r,t)}{\partial r}\right) = \frac{1}{\alpha(t)}\cdot\frac{\partial T(r,t)}{\partial t} \quad (2)$$

within the RPV wall

where, T(r,t) is temperature in the RPV, $T_{wall}(t)$ and $T_{\infty}(t)$ are temperature at the inner surface and coolant temperature, respectively. And k(t), h(t), and $\alpha(t)$ are thermal conductivity, heat transfer coefficient, and thermal diffusivity. Only for a very limited condition, such that $T_{\infty}(t)$ is given as a simple exponential or polynomial function of time for plate geometry, T(r,t) can be found as closed form solutions containing sinusoidal and exponential functions[3]. However, in most practical cases, $T_{\infty}(t)$ may not easily represented as simple exponential or polynomial functions, and

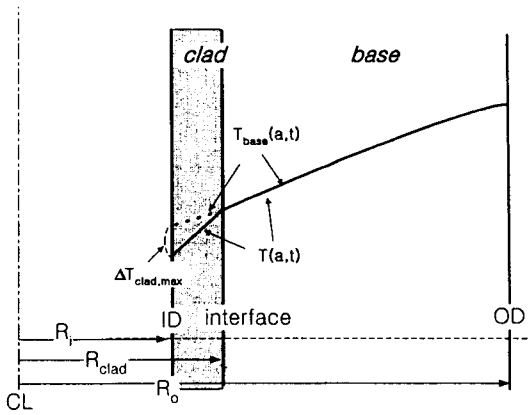

Fig. 2. Separation of Temperature Component into Base Metal and Hypothetical Clad Components

RPV is in cylindrical geometry. For such conditions, closed form solutions to eq. 1) and 2) are unavailable and, therefore, numerical methods like finite element method should be used to found T(r,t). In this study, the numerical solution module of OCA-P code[2] is used to find T(r,t).

Once, the temperature profile, T(r,t) within the vessel is determined, temperature profile was modified as shown in figure 2 to be used in thermal stress calculation. First, the temperature profile in base metal part, $T_{base}(r,t)$, is fitted as a 4-th order polynomial. Because of differences in thermal conductivity and resulting steeper temperature gradient, actual temperature profile in clad would deviate considerably from $T_{base}(r,t)$. Hypothetical temperature at the inner surface, $T_{base}(Ri,t)$ could be found as follows by extending $T_{base}(r,t)$ to the inner wall, as shown in figure 2;

$$T_{base}(R_i,t) = T(R_{clad},t) + \frac{k_{clad}(t)}{k_{base}(t)} \cdot [T(R_i,t) - T(R_{clad},t)] \quad (3)$$

where, $T_{base}(Ri,t)$: hypothetical temperature at inner wall, extrapolated using temperature profile in base metal, $T_{base}(r,t)$

$T(R_i,t)$: true temperature at inner wall

$T(R_{clad},t)$: true temperature at clad/base interface

R_{clad}: radial distance of clad/base interface from center

By doing this, single analytic temperature profile can be used to calculate the thermal stress corresponding to the temperature profile in base metal. To account for the temperature difference in clad and resulting thermal stress in clad, $\Delta T_{clad}(r,t)$ in figure 2 is simplified as follows;

$$\Delta T_{clad}(r,t) = \Delta T_{clad,\max}(t)\cdot(1-\frac{r}{R_{clad}}),$$
for $R_i \le r \le R_{clad}$ or, within cladding
$$= 0,$$
for $R_{clad} \le r$ or, outside cladding (4)

$$\text{where } \Delta T_{clad,\max}(t) = T_{base}(R_i,t) - T(R_i,t) \quad (5)$$

Therefore temperature profile was divided into two parts as follows;

$$T(r,t) = T_{base}(r,t) - \Delta T_{clad}(r,t) \quad (6)$$

2.2. Thermal Stress Analysis

For infinite cylinder with a concentric circular hole, with inner radius R_i and outer radius R_o, with temperature distribution in r-direction given as T(r), thermal stresses are represented as follows;[8]

$$\sigma_z = \frac{E\cdot\alpha}{1-\nu}\cdot[T_0 - T]$$

$$\sigma_r = \frac{E\cdot\alpha}{1-\nu}\cdot[\frac{1-\frac{R_i^2}{r^2}}{2}T_0 - \frac{1}{r^2}\cdot\int_{R_i}^{r} Trdr] \quad (7)$$

$$\sigma_\theta = \frac{E\cdot\alpha}{1-\nu}\cdot[\frac{1+\frac{R_i^2}{r^2}}{2}T_0 + \frac{1}{r^2}\cdot\int_{R_i}^{r} Trdr - T]$$

$$T_0 = \frac{2}{R_o^2 - R_i^2}\cdot\int_{R_i}^{R_o} Trdr \quad (8)$$

When the thickness of cylinder is very small compared to the radius of cylinder, or $R_o \to R_i$, the integral term in the formulas become sufficiently small, and the first approximation of stresses could be; $\sigma_r \sim 0$ and $\sigma_\theta \sim \sigma_z$. Therefore, thermal stress arising from temperature profile in base metal can be simply represented as follows;

$$\sigma_\theta \approx \sigma_Z = \sigma_{base}(r,t) = \frac{E_{base}}{1-\nu_{base}}\cdot(T_0(t) - T_{base}(r,t))\cdot\alpha_{base} \quad (9)$$

where, E_{base} : Young' s modulus of base metal

α_{base}: linear thermal expansion coefficient

ν_{base} : Poisson' s ratio of base metal

Because the temperature within the vessel wall, T(r,t) is represented as 4-th order polynomials, above equation can also be represented as 4-th order polynomial. That is,

$$\sigma_{base}(r,t) = \frac{E_{base}}{1-\nu_{base}}\cdot(T_0(t) - T_{base}(r,t))\cdot\alpha_{base} = \sum_{i=0}^{4} B_i(t)\cdot r^i \quad (10)$$

As shown in eq. 10), coefficients of stress formula are directly derived from those of temperature profile. Once stress distribution from $T_{base}(r,t)$ was determined from eq. 10), additional stress due to the existence of cladding had to be determined. There are two sources of cladding stress. One is the stress from the difference in thermal expansion between clad and base metals, or $\sigma_{clad,\alpha}$. The other is the stress from the difference between real temperature in clad, T(r,t) and hypothetical temperature extrapolated from $T_{base}(r,t)$, or $\sigma_{clad,\Delta T}$.

It is assumed that with proper post-weld heat treatment after welding, RPV shell is free from thermal stress at normal operating temperature of about 288℃.[2] This temperature is defined as the stress-free temperature of cladding, T_{free}, which is usually equal to normal operating temperature

of RPV. When vessel is cooled below the stress free temperature, difference in thermal expansion produces additional tensile stress in clad and compressive stress in base metal. The tensile stress in clad due to the difference in thermal expansion coefficient, $\sigma_{clad,\alpha}$, can be represented as follow;

$$\sigma_{clad,\alpha} = \frac{E_{clad}\cdot\alpha_{clad}}{1-\nu_{clad}}[T_{free}-T(r,t)] - \frac{E_{base}\cdot\alpha_{base}}{1-\nu_{base}}[T_{free}-T(r,t)] \quad (11)$$

If Young' s moduli and Poisson' s ratios of clad and base metals are similar, above equation can be simplified.

$$\sigma_{clad,\alpha} = \frac{E_{clad}\cdot(\alpha_{clad}-\alpha_{base})}{1-\nu_{clad}}\cdot[T_{free}-T(r,t)] \quad (12)$$

The second source of clad stress arises from the temperature difference in clad, $\sigma_{clad,\Delta T}$, can be represented as follows,

$$\sigma_{clad,\Delta T} = \frac{E_{base}\cdot\alpha_{base}}{1-\nu_{base}}\cdot\Delta T_{clad} = \frac{E_{base}\cdot\alpha_{base}}{1-\nu_{base}}\cdot[T_{base}(r,t)-T(r,t)] \quad (13)$$

Therefore, total clad stress in clad is;

$$\sigma_{clad} = \sigma_{clad,\alpha}+\sigma_{clad,\Delta T} = \frac{E_{clad}}{1-\nu_{clad}}\cdot(\alpha_{clad}-\alpha_{base})\cdot[T_{free}-T(r,t)] + \frac{E_{base}\cdot\alpha_{base}}{1-\nu_{base}}\cdot[T_{base}(r,t)-T(r,t)] \quad (14)$$

At vessel inner surface and clad/base interface, clad stress can be calculated from eq. 14), that is,

$$\sigma_{ID} = \frac{E_{clad}}{1-\nu_{clad}}\cdot(\alpha_{clad}-\alpha_{base})\cdot[T_{free}-T_{ID}] + \frac{E_{base}\cdot\alpha_{base}}{1-\nu_{base}}\cdot\Delta T_{clad,max} \quad (15)$$

$$\sigma_{interface} = \frac{E_{clad}\cdot(\alpha_{clad}-\alpha_{base})}{1-\nu_{clad}}(T_{free}-T_{interface})$$

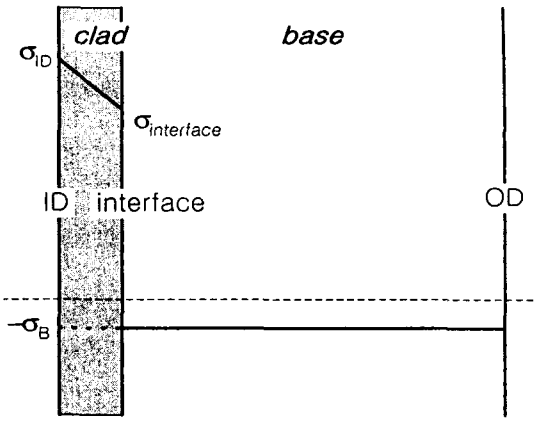

Fig. 3. Clad Stress Distribution Arising from Differences in Thermal Conductivity and Thermal Expansion Coefficients

Because the thickness of cladding is very small, it is possible to assume that the temperature changes linearly and hoop stress is same as axial stress. Further simplification is possible from linear temperature distribution such that, clad stress also varies linearly from σ_{ID} at vessel wall to $\sigma_{interface}$ at clad/base interface[3,9].

The schematic of clad stress distribution is shown in figure 3. Clad stress is an additional stress to be added to the thermal stress produced by temperature profile in base metal. Though the clad stress in clad could be very large, it is confined in very thin layer, compressive stress in base metal would not be significant. The simple approximation could be assumed constant compressive stress in base metal. The resulting stress distribution due to the existence of cladding would be as follows;

$$\sigma_{clad} = \sigma_{ID}\cdot(1-q\cdot\frac{r-R_i}{W}) \quad \text{within clad}$$
$$= -\sigma_B \quad \text{within base} \quad (16)$$

where q = gradient of clad stress in cladding normalized to vessel thickness,
$(\sigma_{ID} - \sigma_{interface})/t_{clad}$
$t_{clad} = (R_{clad} - R_I) / W$

W = thickness of the vessel, R_o - R_i

$-\sigma_B$ = constant compressive stress in base to equilibrate the clad stress in cladding

The magnitude of compressive stress σ_B could be found from the force equilibrium. Or,

$$\int_{R_i}^{R_o} \sigma_{clad} dr = \int_{R_i}^{R_{clad}} \sigma_{ID} \cdot (1 - q \cdot (r - R_i)) dr + \int_{R_{clad}}^{R_o} -\sigma_B \cdot dr = 0 \quad (17)$$

$$\text{Then, } \sigma_B = \int_{R_i}^{R_{clad}} \sigma_{ID} \cdot (1 - q \cdot (r - R_i)) dr \, / [\frac{R_0^2 - R_{clad}^2}{2}]$$

Total thermal stress distribution within the vessel wall could be found by superposing each stress component shown in eq. 10) and 16).

$$\sigma_{thermal} = \sigma_{base} + \sigma_{clad} \quad (18)$$

2.3. Stress Intensity Factor Calculation

Total stress intensity factor (SIF) resulting from the stress distribution given in eq. 18) could be found by calculating corresponding SIF for each stress component. For a given stress distribution, general equation for SIF is given as follows;

$$K = f\sigma\sqrt{\pi a W} \quad (19)$$

where, f = weight function

σ= stress acting on crack line

a = crack depth normalized with thickness, A/W

W = thickness of cylinder

For a stress distribution given as polynomial function, corresponding weight function could be found as follows;

$$\sigma(x) = \sum_{n=0}^{N} C_n x^n \quad (20)$$

where x = (r - R_i)/W, normalized distance

$$f = \sum_{n=0}^{N} C_n f_n \quad (21)$$

The coefficient in eq. 21), f_n could be represented as function of normalized flaw depth, as $f_n(a)$.

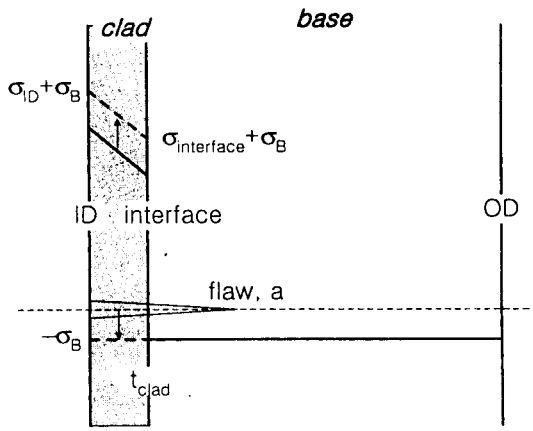

Fig. 4. Modified Clad Stress Distribution to Calculate SIF Acting at Crack Tip Located in Base Metal

$$f_n(a) = \sum_{i=0}^{I} \alpha_i a^i \quad (22)$$

$f_n(a)$ depends on variety of factors like geometry, flaw orientation, and flaw depth. Sometimes, it is convenient to use the coefficients normalized to flaw depth.

$$\frac{f_n(a)}{a^n} = F_n = \sum_{i=0}^{I} \frac{\alpha_i}{a^n} a^i = \sum_{i=0}^{I} \beta^i a^i \quad (23)$$

In this case eq. 19) could be rewritten as follows;

$$K = \sqrt{\pi a W} \cdot \sum_{n=0}^{N} C_n F_n a^n \quad (24)$$

where, C_n is the coefficient of each term in stress distribution shown in eq. 10), and F_n is defined as influence coefficient for each term in stress distribution. For an infinitely long eccentric cylinder with radius to thickness ratio (R/t) of 10, influence coefficients are given as fourth-order polynomials[3,9];

- for infinite long axial flaw located on inner surface

$$\begin{aligned} F_0(a) &= 1.1220 + 0.9513 \cdot a - 0.6240 \cdot a^2 + 8.3306 \cdot a^3 \\ F_1(a) &= 0.6825 + 0.3704 \cdot a - 0.0832 \cdot a^2 + 2.8251 \cdot a^3 \\ F_2(a) &= 0.5255 + 0.2011 \cdot a + 0.0313 \cdot a^2 + 1.4250 \cdot a^3 \\ F_3(a) &= 0.4414 + 0.1337 \cdot a + 0.0386 \cdot a^2 + 0.8806 \cdot a^3 \\ F_4(a) &= 0.3863 + 0.0989 \cdot a + 0.0437 \cdot a^2 + 0.5951 \cdot a^3 \end{aligned} \quad (25)$$

- for continuous circumferential flaw located on inner surface

$$F_0(a) = 1.1220 + 0.3989 \cdot a + 1.5778 \cdot a^2 + 0.6049 \cdot a^3$$
$$F_1(a) = 0.6830 + 0.1150 \cdot a + 0.7556 \cdot a^2 + 0.1667 \cdot a^3$$
$$F_2(a) = 0.5260 + 0.1911 \cdot a - 0.1000 \cdot a^2 + 0.5802 \cdot a^3 \quad (26)$$
$$F_3(a) = 0.4450 + 0.0783 \cdot a + 0.3148 \cdot a^2 + 0.4414 \cdot a^3$$
$$F_4(a) = 0.3880 + 0.1150 \cdot a - 0.1333 \cdot a^2 + 0.3519 \cdot a^3$$

Using above equations, SIF corresponding to 4-th order polynomial stress distribution in base metal, K_{base} can be easily calculated. However, finding SIF from clad stress would be quite complicated. When the crack tip is confined within the cladding where clad stress was given as linear function, $F_0(a)$ and $F_1(a)$ in above equation can be used to calculated SIF acting on the crack tip.

$$K_{clad} = \sqrt{\pi a W} \cdot \sigma_{ID} \cdot [F_0(a) - q \cdot a \cdot F_1(a)] \quad (27)$$

On the other hand, when crack tip is located in base metal, clad stress distribution is modified as shown in figure 4. For segment of crack in cladding, effective stress on crack plane is increased to $\sigma_{clad} + \sigma_B$. Then, to compensate the increased stress in cladding, compressive stress $-\sigma_B$ is extended to the inner surface of cladding. SIF acting at crack tip from each stress distribution can be separately calculated and summed together to calculate total SIF acting at crack tip.

From figure 4, effective clad stress in cladding σ_{clad}^* is defined as follows;

$$\sigma^*_{clad} = \sigma_{clad} + \sigma_B = \sigma_{ID} \cdot (1 + \frac{\sigma_B}{\sigma_{ID}} - q \cdot a) \quad (28)$$

And, corresponding SIF is,

$$K^* = f \cdot \sigma^*_{clad} \cdot \sqrt{\pi \cdot a \cdot W}$$
$$f = (1 + \frac{\sigma_B}{\sigma_{ID}}) \cdot f_c - q \cdot a \cdot f_l \quad (29)$$

Influence coefficient f_c and f_l are function of geometry, flaw orientation, flaw size, and additionally, ratio of clad thickness to thickness of cylinder. Using tables and methods provided in reference[5], influence coefficient for an eccentric cylinder with thickness to radius ratio of approximately 1/10 are determined as follows[9];

$$\log_{10}(f_{coj}(a) \cdot \sqrt{a}) = \sum_{k=0}^{6} h_{cojk} \cdot (\log_{10} a)^k \quad (30)$$

$$\log_{10}(f_{loj}(a) \cdot \sqrt{a}) = \sum_{k=0}^{6} h_{lojk} \cdot (\log_{10} a)^k \quad (31)$$

where h_{cojk} and h_{lojk} are correlation coefficients. From eq. 30) and 31), f_c and f_l for given flaw orientation and clad thickness to vessel thickness ratio are calculated. For normalized clad thickness t_{clad} ranging from 0.01 to 0.04, corresponding influence coefficients can be calculated by interpolating neighboring values from above equations. The detailed description of above equations is shown in elsewhere[9]. For a constant stress acting on the whole length of crack, corresponding SIFs can be easily calculated from the influence coefficient $F_0(a)$ in eq. 25) and 26).

$$K_B = -F_0(a) \cdot \sigma_B \cdot \sqrt{\pi \cdot a \cdot W} \quad (32)$$

Therefore, SIF acting on the crack tip located in the base metals arising from clad stress can be calculated as the sum of K^* and K_B. In all, total SIF associated with temperature profile, T(r,t) could be found by superposing individual SIF for each stress distribution.

$$K_{thermal} = K_{base} + K_{clad} \quad \text{for } a \le t_{clad}$$
$$= K_{base} + K^* + K_B \quad \text{for } a \ge t_{clad} \quad (33)$$

Above methodology to calculate thermal SIF considering the stainless cladding has been incorporated into the existing PFM code[3] to develop improved PFM code[10].

Table 1. Geometry of Vessel

Model plant	Hypothetical Vessel
Vessel Inner Radius	2184 mm
Vessel Thickness	216 mm
Cladding Thickness	5.4 mm

2.4. Critical RTNDT Analysis

According to the classical linear elastic fracture mechanics, flaws will begin to initiate when applied SIF exceeds K_{IC} calculated from the lower-bound fracture toughness curve. The conservative lower-bound KIC curve can be determined from T and RT_{NDT}(reference temperature-nil ductility transition) using the following equation given in ASME Section XI, Appendix A[11];

$$K_{IC} = 36.52 + 22.81 \cdot \exp[0.036 \cdot (T - RT_{NDT})] \quad (34)$$

in $\mathrm{MPa}\sqrt{\mathrm{m}}$

Several studies have shown that the fracture toughness can be significantly increased at low temperatures if the material is prestressed at higher temperatures[12, 13]. A simple method to use the basic premise of warm prestressing effect in the fracture mechanics of pressure vessels under thermal shock is that a crack will not initiate when the stress intensity factor is dropping with time or constant[14].

3. Reference Transient and Analysis Cases

The reference transient to evaluate the effects of stainless cladding is selected from the PTS transients used in EPRI-sponsored PTS benchmarking evaluation[15]. During the transient, temperature decreases exponentially from 288℃ to 66℃ with rate of -0.05℃ / min. Heat transfer coefficient at the inner surface of

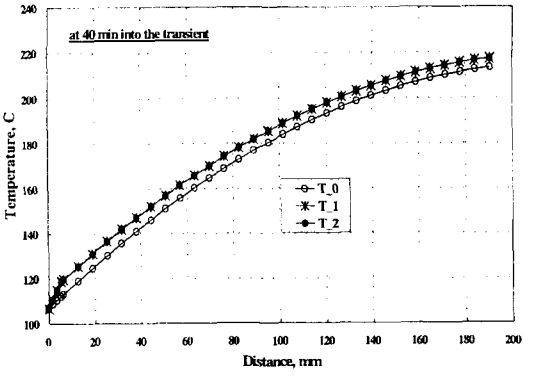

Fig. 5. Modified Clad Stress Distribution to Calculate SIF Acting at Crack Tip Located in Base Metal

vessel is assumed constant at 1810 W/m^2-K throughout the transient. Pressure is maintained at 138 MPa throughout the transient. The geometry of the RPV is summarized in table 1. The thermo-physical and mechanical properties of RPV are summarized in table 2. The effect of cladding is evaluated for 3 cases as follows;

Case 0 : No cladding. Clad properties are assumed as identical to base metal.

Case 1 : Clad thermal conductivity is considered. Additional stress from steep temperature gradient in clad is evaluated.

Case 2 : Clad is fully considered. Additional stress from steep temperature gradient and differential thermal expansion are evaluated.

As a measure to evaluate the impacts of the cladding treatment in PTS analysis, the critical RT_{NDT} for flaw initiation are calculated for 6.35 mm (0.25″) deep (crack tip is located at just outside of the clad) and 12.7 mm (0.5″) deep flaws. The critical RTNDT for flaw initiation for the following cases are calculated;

- When WPS(warm pre-stressing) effect is not considered : the lowest RT_{NDT} whose lower-bound K_{IC} curve meets the applied SIF curve.

Table 2. Materials Properties of Base and Clad Metals for Fracture Mechanics Analysis

	Case 0	Case 0	Case 1	Case 2
Material Property	Base & Weld	Stainless Steel Cladding		
Thermal Conductivity, W/m-°K	41.5	41.5	17.3	17.3
Specific Heat, J/Kg-°K	502.4	502.4		
Density, Kg/m^3	7833	7833		
Modulus of Elasticity, GPa	193	193		
Thermal Expansion Coefficient, m/m-°K	1.53E-5	1.53E-5	1.53E-5	1.8E-5
Poisson' s Ratio	0.3	0.3		

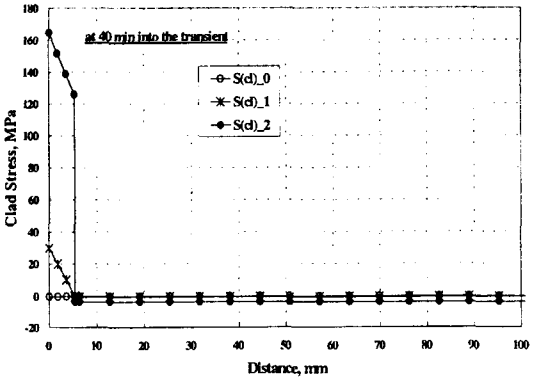

Fig. 6. Comparison of Clad Stress on Infinite Axial Crack Tip Within Vessel at 40 Minutes into the Transient

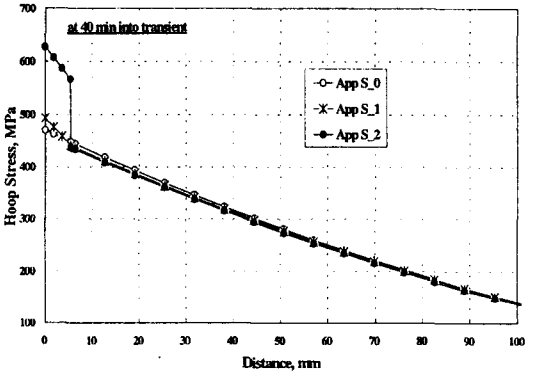

Fig. 7. Comparison of Hoop Stress at 40 Minutes into the Transient

- When WPS effect is considered: the RT_{NDT} whose lower-bound K_{IC} curve meets the maximum applied SIF.

4. Results and Discussion

4.1. Thermal and Stress Analysis

Temperature profiles at 40 minutes into the transient are shown in figure 5. As expected, Case 1 and 2 that incorporated clad thermal conductivity, show identical temperature profiles. Meanwhile, Case 0, in which clad thermal conductivity is not considered, produced about 5℃ lower temperature within the vessel. For highly embrittled vessels, such seemingly small temperature differences could have larger effects on fracture toughness, especially around mid-transition temperature.

Clad stresses from the existence of stainless steel at 40 minutes into transient are shown in figure 6. Case 1, in which clad thermal conductivity is considered, showed increased tensile stress within the clad. By comparing Case 1 with Case 2, it is clear that the contribution of differential thermal expansion between clad and base is far greater than that of difference in thermal conductivity. Total hoop stresses at 40 minutes into the

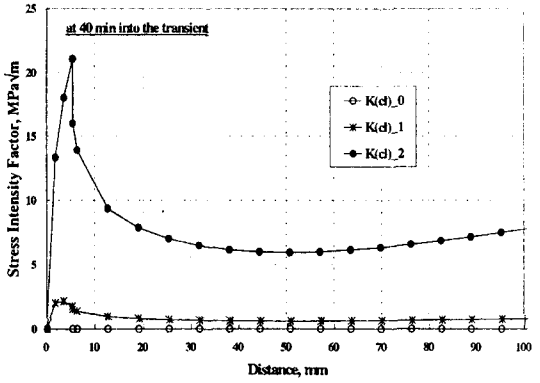

Fig. 8. Comparison of SIFs form Clad Stress Within Vessel at 40 Minutes into the Transient

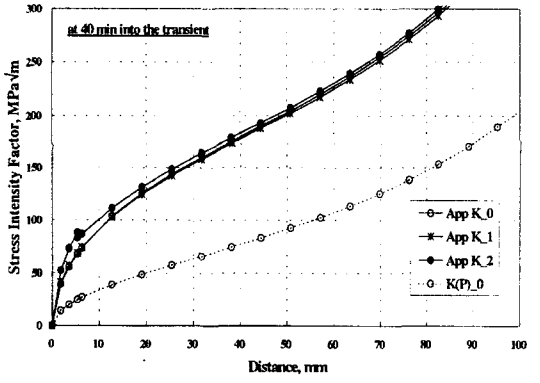

Fig. 9. Comparison of Applied SIF(including SIF from pressure loading, shown as dotted line) from All Source of Stress on Infinite Axial Crack Tip Within Vessel at 40Minutes into the Transient

transient, along with stress from pressure loading are shown in figure 7. As shown in the figure, tensile stress in clad region for Case 2 is substantially higher than those for other cases mainly because larger thermal expansion coefficients of stainless steel cladding is fully considered. In this case, however, resulting stress is lower within the base metal part of the vessel. It should be mentioned that in VISA-II code, only the first term in eq. 14) is considered and resulted

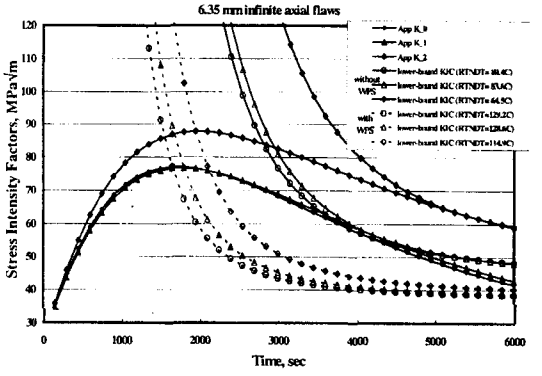

Fig. 10. Applied SIFs and Lower-Bound KIC Curves at 6.35mm Infinite Axial Crack Tip at the Event PTS Tansient

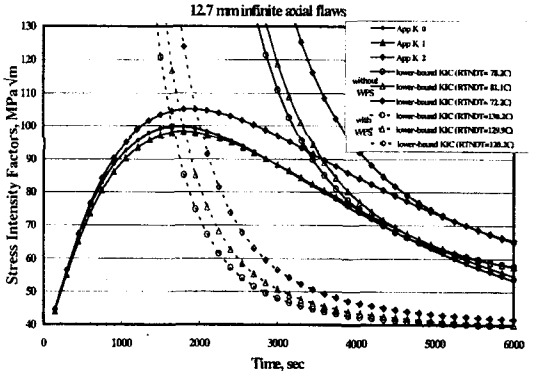

Fig. 11. Applied SIFs and Lower-Bound K_{IC} Curves at 12.7mm Deep Infinite Axial Crack Tip at the Event of PTS Transient

in lower stress in the clad compared to FAVOR code that simultaneously considered both terms in the equation. The comparison of current methodology with other PFM codes are provided elsewhere[10].

4.2. Stress Intensity Factor Calculation

The SIF calculations for the clad stress at 40 minutes into transient provided in previous section are shown in figure 8. Like stress distribution in figure 6, SIF for Case 2 is far greater than the

Table 3. Critical RT_{NDT}s at 6.35 mm Deep Crack Tip for Flaw Initiation During Reference Transient(in℃)

	Axial Flaws		Circumferential Flaws	
	Without WPS	With WPS	Without WPS	With WPS
Case 0	80.4	129.2	104.6	142.4
Case 1	83.6	128.6	108.6	142.0
Case 2	64.5	114.9	84.5	124.8

Table 4. Critical RT_{NDT}s at 12.7 mm Deep Crack Tip for Flaw Initiation During Reference Transient(in℃)

	Axial Flaws		Circumferential Flaws	
	Without WPS	With WPS	Without WPS	With WPS
Case 0	78.2	130.2	98.6	141.1
Case 1	81.1	129.9	102.6	141.1
Case 2	72.2	120.2	91.4	130.1

others, especially near the clad/base interface. It is especially significant that the flaw existence probabilities are greater in these flaw sizes[3]. Overall SIFs acting on the tip of the infinite axial flaws are shown in figure 9. As shown in the figure, in the range of flaw depth 3 mm to 20 mm, Case 2 shows about 5 to 15 MPa(m higher applied SIF. By comparing the SIFs for Case 0 and Case 1, it could be said that the effect of the differences in thermal conductivity alone is not so significant.

4.3. Critical RT_{NDT} Analysis

The applied SIF acting on the tip of 6.35 mm and 12.7 mm deep surface flaws along with corresponding lower-bound K_{IC} curves are shown in figures 10 and 11. For 6.35 mm deep flaws, the SIF for Case 2 are significantly greater (at least 10 MPa$\sqrt{m}$ after reaching peak SIF values) than those for Case 0 and Case 1. As flaw size increases from 6.35 mm to 12.7 mm, the difference in the applied SIFs become smaller. Similar results are observed for the continuous circumferential flaws.

Critical RT_{NDT}s for flaw initiation are estimated and summarized in tables 3 and 4. As expected from the figures 10 and 11, the critical RT_{NDT}s for Case 0 and 1 are similar, differing only a few degree. However, it should be noted that considering only the thermal conductivity of the stainless cladding, like Case 1, results in the least conservative critical RT_{NDT}. On the other hand, Case 2 showed lowest critical RT_{NDT}s of the three cases. As the flaw size increases from 6.35 mm to 12.7 mm, the differences in critical RT_{NDT}s for Case 1 and Case 2 decrease from about 20℃ to 10℃, confirming that the effect of cladding become smaller as the flaw size increases.

As shown in table 3, the incorporation of WPS effect in PTS analysis decreases the differences in RT_{NDT}s of 6.35 mm flaws for Case 1 and Case 2 (from 19.1℃ to 13.7℃ for axial flaw and from 24.1℃ to 17.2℃ for circumferential flaw). It also

makes the differences in the critical RT_{NDT}s for Case 0 and 1 become even smaller, differing less than a degree for both flaw depths and orientations the for 6.35 mm deep flaws.

5. Summary and Conclusions

The existence of cladding on the inner surface of reactor pressure vessel makes the temperature, stress, and stress intensity factor calculation during pressurized thermal shock transients complicated. A simple treatment method is developed to deal with clad induced stress and stress intensity factors.

The thermal stress is divided into stress from base metal temperature distribution and one from the existence of cladding. Clad stress arises due to the difference in thermal conductivity and thermal expansion coefficient between the base and clad materials. Clad stress is further divided into linearly varying stress component in clad and constant compressive stress in base metal. Consequently, applied stress intensity factors due to both stress components are independently calculated and added to find total stress intensity factors.

The stress intensity factor from clad stress is calculated as follows;.

- For crack within clad, SIFs are calculated for the clad stress distribution
- For crack outside clad, SIFs from clad stress and compressive stress in base are added.

Once the treatment method is developed, the effect of clad on the deterministic analysis for a hypothetical PTS transient is examined and the followings are observed;

- When the differences in thermal conductivity and thermal expansion coefficients of stainless clad are fully incorporated, resulting stress is higher within the clad, but lower within the base metal part of the vessel.
- When clad is fully considered, the applied SIFs are significantly greater, but as flaw size increases, the difference in the applied SIFs become smaller. Similar results are observed for the continuous circumferential flaws.

Finally, the effects of clad on the critical RT_{NDT} for flaw initiation for 6.35 mm and 12.7 mm deep flaws are analyzed and the followings are observed;

- The critical RT_{NDT}s for flaw initiation is the lowest when clad is fully considered. However, as the flaw size increases from 6.35 mm to 12.7 mm, the differences in the critical RT_{NDT}s for Case 1 and Case 2 decrease from about 20℃ to 10℃, confirming that the effect of cladding become smaller as the flaw size increases.
- When warm pre-stressing effect is considered, the effect of cladding treatment method on critical RT_{NDT}s becomes less significant for the short flaws like 6.35 mm flaws.

References

1. USNRC, "NRC Staff Evaluation of Pressurized Thermal Shock," SECY 82-465(1982).
2. R. D. Cheverton and D. G. Ball, "OCA-P, A Deterministic and Probabilistic Fracture-Mechanics Code for Application to Pressure Vessels," NUREG/CR-3618(1984).
3. F. A. Simonen et al. "VISA-II, A Computer Code for Predicting the Probability of Reactor Vessel Failure," NUREG/CR-4486(1986).
4. T. L. Dickson, "FAVOR: A Fracture Analysis Code for Nuclear Reactor Pressure Vessels, Release 9401," ORNL/NRC/LTR/94/1 (1994).
5. X. R. Wu and A. J. Carlsson, "Weight Functions and Stress Intensity Factor Solutions," Pergamon Press, New York(1991).
6. T. Fett and D. Munz, "Stress Intensity Factors and Weight Functions," Computational

Mechanics Publication, Boston(1997).
7. C. H. Jang, et. al, Comparative Study of Probabilistic Fracture Mechanics Codes, in the proceedings of the KNS '99 spring meeting, Pohang, Korea, May 28 - 29(1999).
8. S. P. Timoshenko and J.N. Goodier, "Theory of Elasticity," McGraw-Hill Company, New York(1970).
9. C. H. Jang, "Treatment of Cladding in Pressurized Thermal Shock Evaluation," KEPRI TM.96NJ12.P1998.898(1998).
10. C. H. Jang, "Development of Probabilistic Fracture Mechanics Analysis Code: KAPTS-KEPRI Analysis of Pressurized Thermal Shock," KEPRI TM.97NJ26.P1999.511 (1999).
11. ASME, "Analysis of Flaws," Nonmandatory Appendix A to ASME Boiler and Pressure Vessel Code, Section XI(1998).
12. J. J. McGowan, Application of Warm Prestressing Effects to Fracture Mechanics Analyses of Nuclear Reactor Vessels during Severe Thermal Shock, Nuclear Engineering and Design, Vol. 51, pp. 431-444(1979).
13. D. A. Curry, A model for Predicting the Influence of Warm Pre-stressing and Strain Aging on the Cleavage Fracture Toughness of Ferritic Steels, International Journal of Fracture, Vol. 22, pp. 145-159(1983).
14. M. J. Jhung, Y. W. Park, and C. H. Jang, Pressurized Thermal Shock Analyses of A Reactor Pressure Vessel Using Critical Crack Depth Diagram, Int. J. of Pressure Vessels and Pipings, Vol. 76, pp. 813-823(1999).
15. K. Balkey et al., "Documentation of Probabilistic Fracture Mechanics Codes Used for Reactor Pressure Vessels Subjected to Pressurized Thermal Shock Loading," EPRI TR-105001(1995).